Supporting Information

ALD-based hydrothermal facile synthesis of dense WO_3@TiO_2-Fe_2O_3 nanodendrite array with enhanced photoelectrochemical properties

Kai-Ping Yuan[ab], Li-Yuan Zhu[a], Qi Cao[c], Hong-Ping Ma[a], Jia-Jia Tao[a], Wei Huang[a], Hong-Liang Lu[*,a]

[a] *State Key Laboratory of ASIC and System, School of Microelectronics, Fudan University, Shanghai 200433, China*

[b] *Department of Electronic Engineering, Fudan University, Shanghai 200433, China*

[c] *Key Laboratory of Energy Thermal Conversion and Control of Ministry of Education, School of Energy and Environment, Southeast University, Nanjing 210096, China*

E-mail: honglianglu@fudan.edu.cn

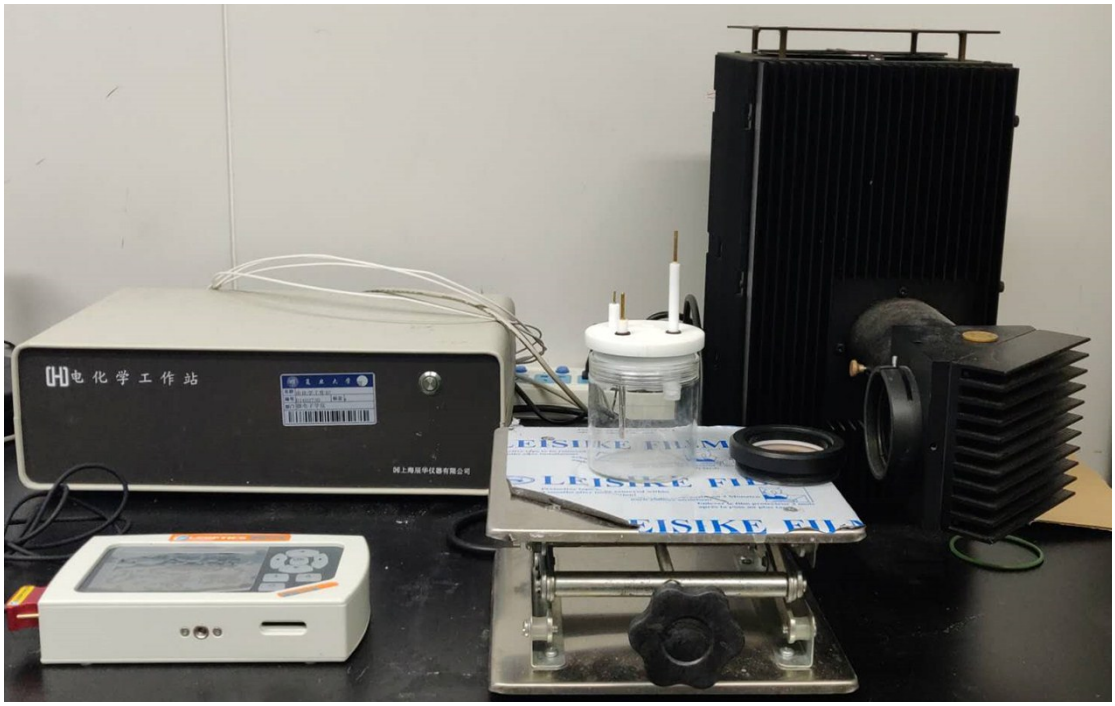

Figure S1. The digital photo of electrochemical measurement set-up

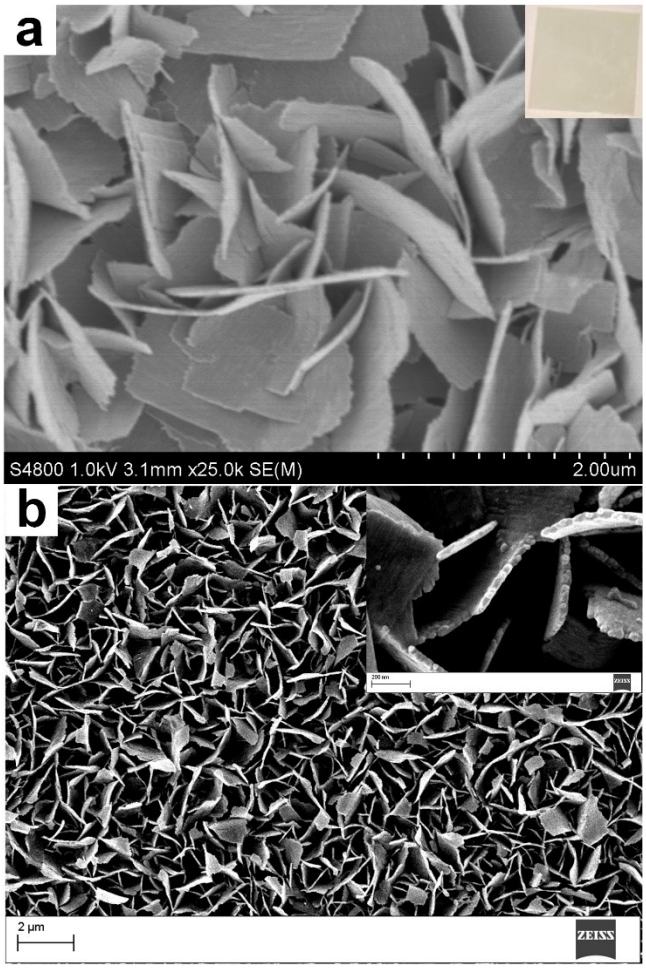

Figure S2. SEM images of as-obtained (a) pure WO_3 nanosheets and (b) WO_3@TiO_2(11 nm) core shell nanosheets array. Inset in (a) is the digital photograph of pure WO_3 nanosheets array; inset in (b) is the high-magnification SEM image of WO_3@TiO_2(11 nm) core shell nanosheets array.

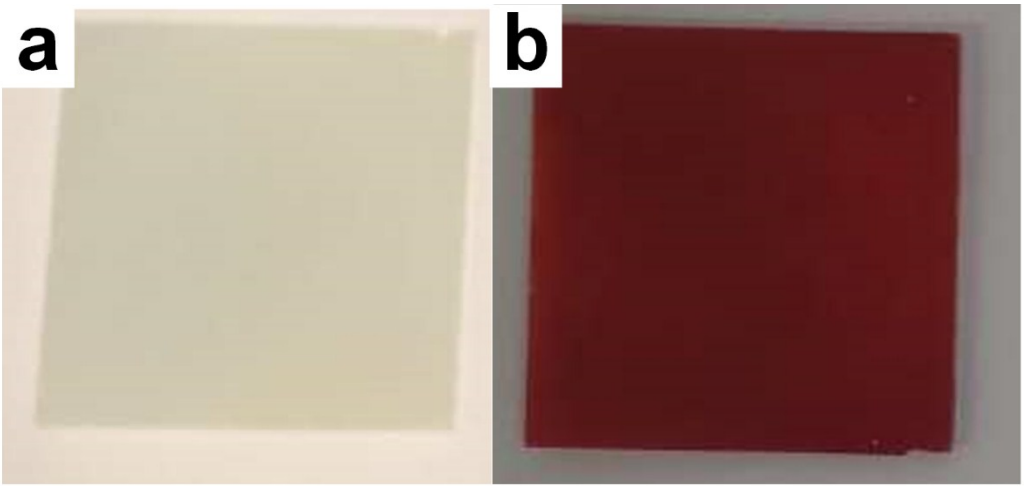

Figure S3. Digital photographs of as-prepared (a) WO_3@TiO_2(11 nm) core-shell nanosheets array and (b) WO_3@TiO_2(11 nm)-Fe_2O_3 nanotrees array.

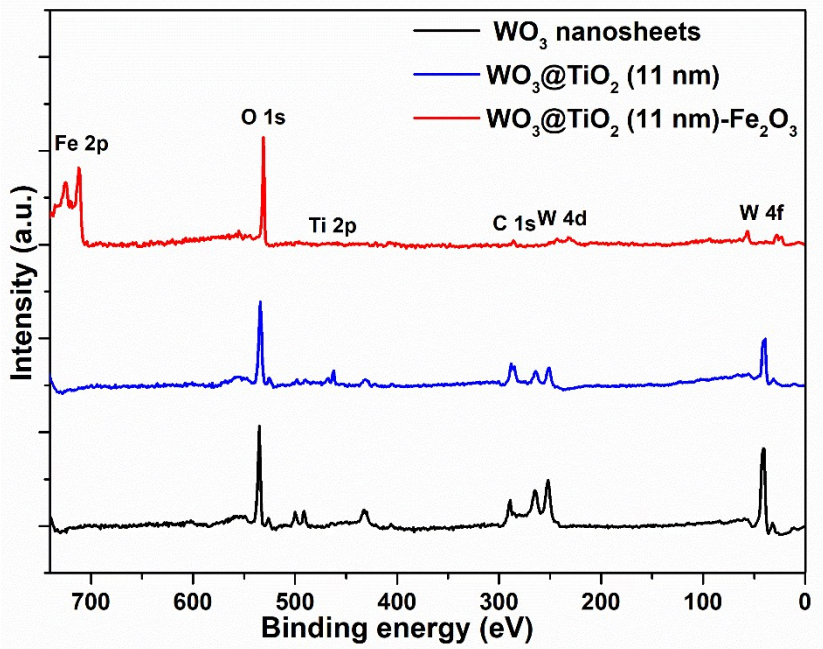

Figure S4. XPS full spectra of the different samples including pure WO_3 nanosheets arrays, WO_3@TiO_2(11 nm) core-shell nanosheets, and WO_3@TiO_2(11 nm)-Fe_2O_3 nanotrees arrays.

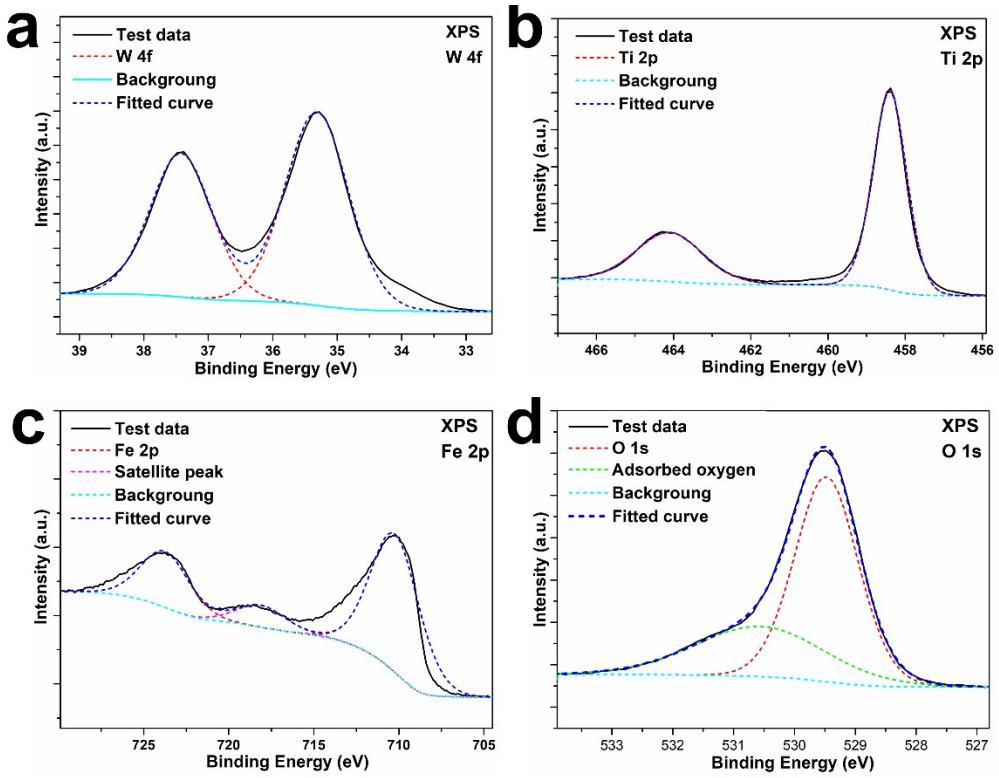

Figure S5. (a) XPS W 4f spectrum of WO_3 nanosheets; (b) XPS Ti 2p spectrum of WO_3@TiO_2 (11 nm); (c) XPS Fe 2pspectrum and (d)XPS O 1s spectrum of WO_3@TiO_2 (11 nm)-Fe_2O_3.

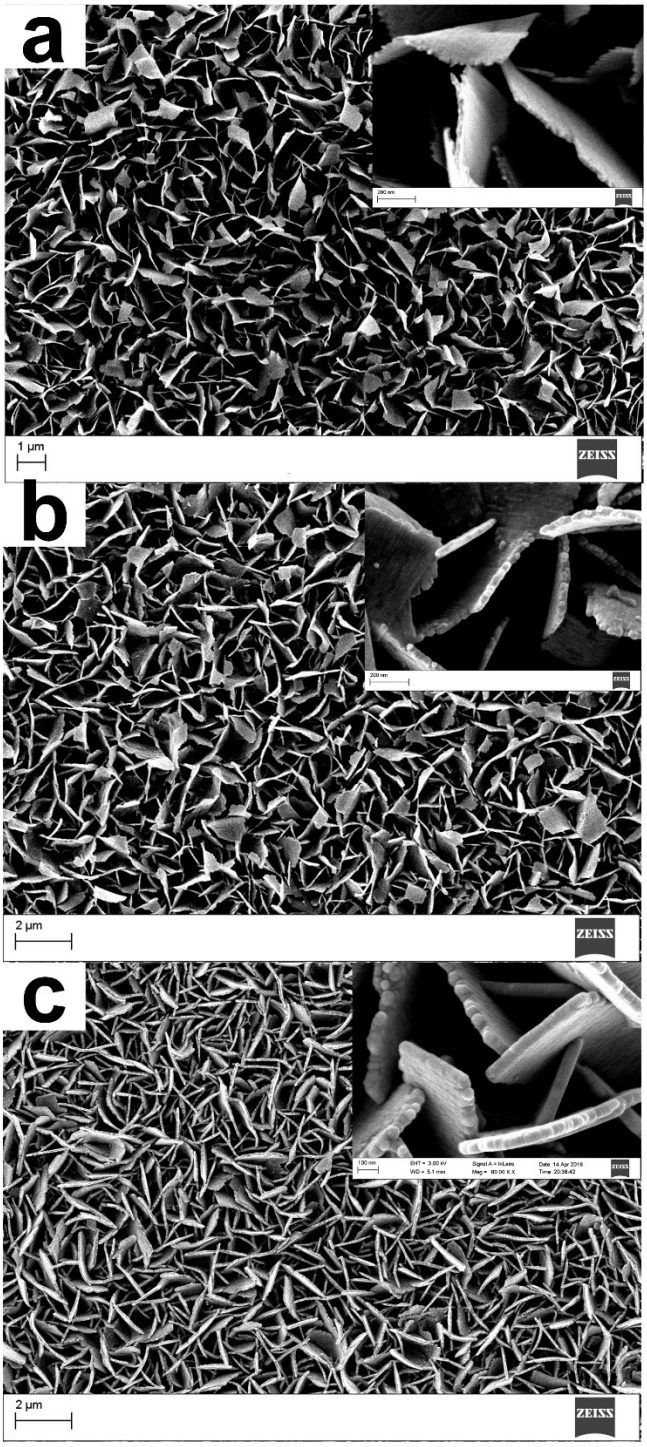

Figure S6. (a-c) Low-magnification SEM images of the obtained WO_3@TiO_2 core-shell nanosheets sample (a) WO_3@TiO_2(5 nm), (b) WO_3@TiO_2 (11 nm) and (c) WO_3@TiO_2(30 nm). Inset in panel a-c are corresponding high-magnification SEM images of the obtained WO_3@TiO_2 core-shell nanosheets.

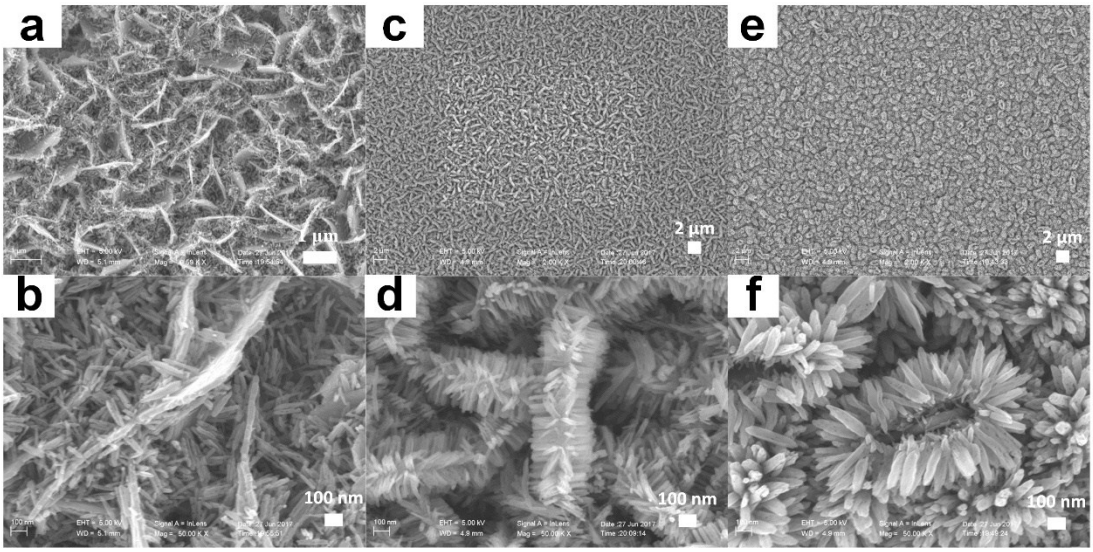

Figure S7. SEM images of WO_3@TiO_2-Fe_2O_3 obtained after 3 h hydrothermal reaction with different thicknesses of the TiO_2 ALD layer: (a-b) 5 nm; (c-d) 11 nm; (e-f) 30 nm.

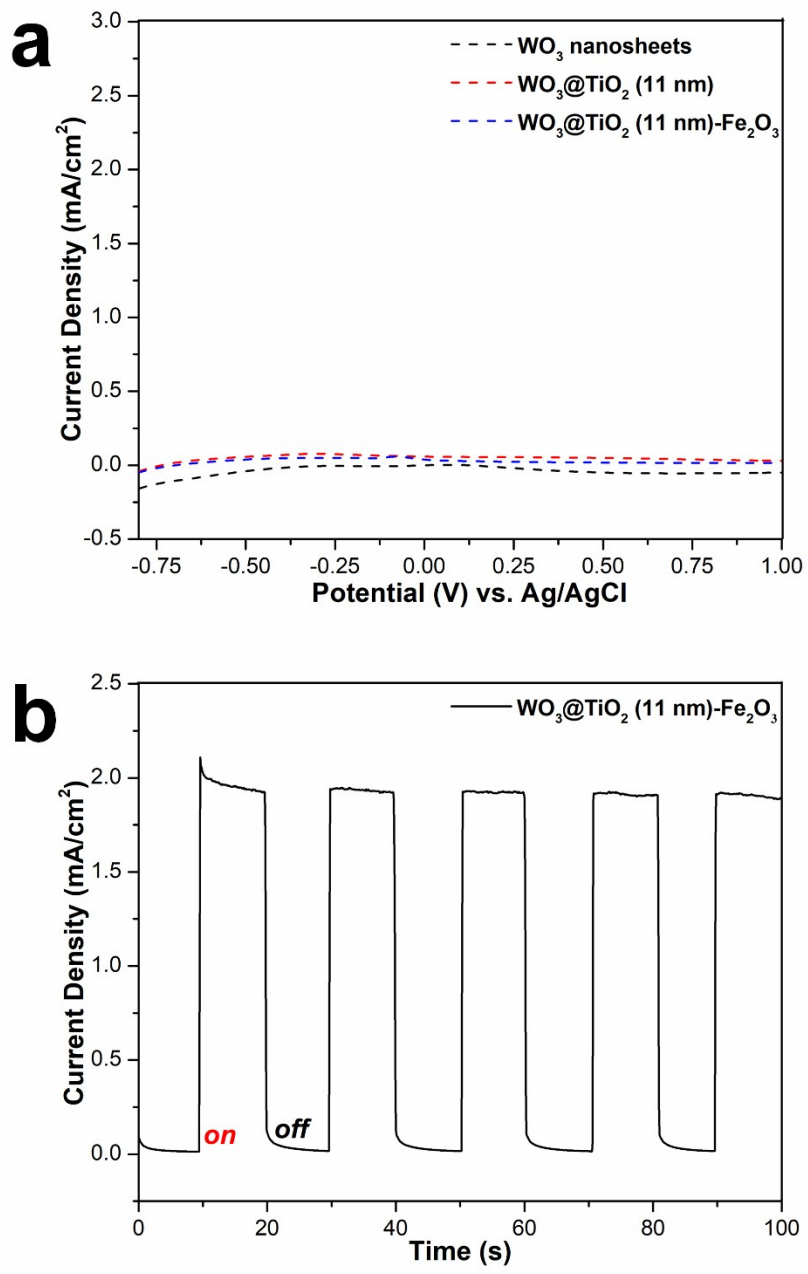

Figure S8. (a) The dark current densities of the the different samples including pure WO_3 nanosheets arrays, WO_3@TiO_2(11 nm) core-shell nanosheets and WO_3@TiO_2(11 nm)-Fe_2O_3 nanotrees arrays; (b) chronoamperometric I-t curves for WO_3@TiO_2(11 nm)-Fe_2O_3 nanotrees arrays photoanode collected at 1.23 V vs. RHE with repeated on-off cycles.

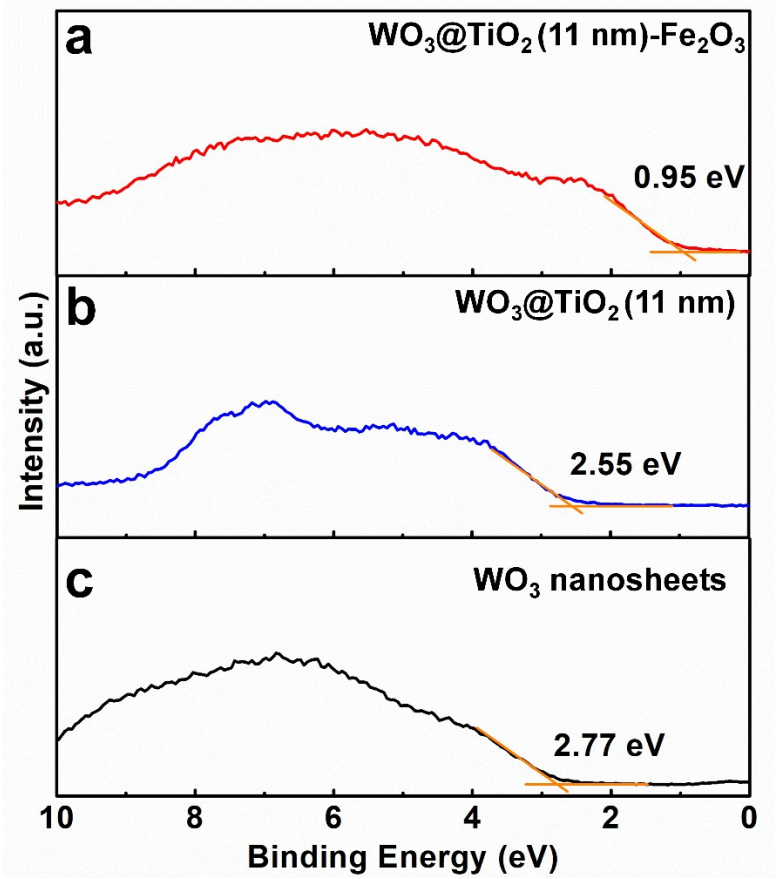

Figure S9. The XPS valence band spectra of the (a) WO_3@TiO_2 (11 nm)-Fe_2O_3., (b) WO_3@TiO_2 (11 nm) and (c) WO_3 nanosheets.